Polymer Journal, Vol. 17, No. 1, pp 225—238 (1985)

Light Scattering Studies of Polymer Solutions and Melts*

Benjamin CHU

Departments of Chemistry and of Materials Science and Engineering,
State University of New York, Stony Brook,
New York 11794-3400, U.S.A.

(Received July 16, 1984)

ABSTRACT: Static and dynamic properties of polymer solutions and melts can be investigated by means of modern scattering techniques. While small angle X-ray scattering (SAXS) and small-angle neutron scattering (SANS) have made advances particularly in studies related to the static structure factor $S(K)$, laser light scattering including the use of Fabry–Perot interferometry and photon correlation spectroscopy has become a standard tool in studying polymer molecular motions. In polymer solutions, the main technique is to use measurements of angular distribution of integrated scattered intensity by means of visible light, SAXS or SANS for $S(K)$ and measurements of angular distribution of the spectrum of scattered light by means of photon correlation spectroscopy for the dynamic structure factor, $S(K, \omega)$. Recent advances have been made in the method of data analysis related to the ill-posed Laplace inversion problem. The new approaches include the singular value decomposition technique and methods of regularization with different criteria for the smoothing operator. By combining static and dynamic light scattering measurements with appropriate algorithms for the Laplace inversion of the time correlation function, a new analytical technique has been developed for polymer molecular weight characterizations. The non-intrusive method has been applied to determine the molecular weight distributions of linear and branched polyethylene in 1,2,4-trichlorobenzene at 135°C and of poly(1,4-phenyleneterephthalamide) in concentrated sulfuric acid. In addition, a new prism light scattering cell is being developed to integrate the above capabilities with chromatographic and other separation techniques. Aside from translational motions of the center of mass of polymers in dilute solution, photon correlation spectroscopy also permits us to investigate rotational, flexual and internal segmental motions. Polymer molecules entangle in semidilute solution. Light-scattering spectroscopy measures a cooperative diffusion coefficient and a slow mode which has been shown to be different in magnitude from the self-diffusion coefficient. The entanglement behavior varies from coils to rod-like polymers. Static and dynamic properties of polymer solutions in semidilute and semiconcentrated regimes can be related to those of bulk polymer melts where measurements of polarized Rayleigh–Brillouin spectra and depolarized Rayleigh spectra yield information on localized structural relaxation and collective segmental/molecular orientational motions. Relaxation times covering a very broad frequency range will be discussed.

KEY WORDS Light Scattering / Polymer Dynamics / Photon Correlation / Interferometry / Melts / Molecular-Weight Distribution /

In the low K regime, the long probing wavelength of visible light, such as $\lambda_0 = 632.8$ nm from a He–Ne laser, permits us to reach macroscopic spatial length scales with $K[=(4\pi n/\lambda_0)\sin(\theta/2)]$ of the order of 10^4 cm^{-1}. If we change the probing radiation to X-rays or neutrons, the much shorter X-ray or neutron wavelengths, of the order of angstroms, cannot reach a comparably low K value by decreasing the scattering angle with $\theta \sim 10^{-3}$ radians. Thus, by combining angular distribution of light scattering intensity measurements with small angle X-ray scattering (SAXS) and small angle neutron scattering (SANS), the static structure factor $S(K)$ can be measured over a large range of spatial scales from atomic spacings to micron sizes.

The dynamic structure factor can also be measured using visible light, X-rays or neutrons. In SANS, only the spin echo technique[1] offers suf-

ficient high resolution and covers a time scale comparable to polymer dynamics. Time-resolution experiments using the X-ray synchrotron radiation[2] have also been performed on a wide variety of dynamic phenomena including those related to polymer systems, such as the kinetics of ligand binding in proteins. However, the temporal and spectral properties of X-ray synchrotron radiation have barely been utilized in SAXS for studies of polymer dynamics. In this article, we are concerned mainly with laser light scattering[3,4] including the use of Fabry–Perot interferometry and photon correlation spectroscopy for investigating polymer molecular motions in solutions and melts.

Many aspects of laser light scattering have been discussed in a series of NATO ASI's on photon correlation and scattering techniques.[5-8] Parallel to the NATO ASI's, there have also been conferences on photon correlation techniques in fluid mechanics.[9] Light-scattering spectroscopy has been made into a powerful routine method for studying the dynamics of polymer solutions[10,11] and melts.[12,13] Instrumentation in photon correlation spectroscopy has been well developed.[14] The only recent modification being the availability of dual delay time increments for a single-clipped correlator[15] and of commercial digital correlators with logarithmically spaced or variable delay time increments so as to increase the bandwidth of the measured time correlation function without increasing the available number of correlator channels. With applications of the singular value decomposition technique and the method of regularization to the ill-posed Laplace inversion problem,[16] we are able to retrieve characteristic delay time distributions of interest from the measured band-width limited time correlation function which contains noise. Under favorable conditions, we are able to estimate the characteristic delay time distribution without an *a priori* assumption on its form. Thus, information other than the average characteristic delay time becomes accessible.

In dilute solutions, measurements of angular distribution of absolute scattered intensity and of time correlation functions permit us to characterize a variety of polymers which are often difficult to investigate because of experimental obstacles. For example, polyethylene is soluble in trichlorobenzene only at high temperatures ($\sim 130°C$) and poly(1,4-phenylene terephthalamide)/PPTA is soluble in concentrated sulfuric acid. Brief outlines of the characterization procedures are presented here in order to show that laser light scattering is a complementary analytical technique to many of the more standard methods, such as osmometry, ultracentrifugation and size exclusion chromatography.

In semidilute solutions, two characteristic decay times have been observed: a fast cooperative diffusion coefficient D_c and a slow-mode diffusion coefficient D_{slow}, which has been found to mimic properties of the self-diffusion coefficient D_s. A brief review of its present status and the interconnection of diffusive motions in semidilute solutions, gels and polymer melts will be presented.

Finally, for bulk polymer melts, measurements of polarized Rayleigh-Brillouin spectra and depolarized Rayleigh spectra by means of Fabry–Perot interferometry and polarized Rayleigh spectra by means of photon correlation spectroscopy will yield information on localized structural relaxation, collective segmental/molecular orientational motions and dynamics of concentration fluctuations. Implications of an extremely broad distribution of relaxation times will be discussed. In my presentation, I emphasize only recent developments, mostly performed by my research group, partly because reviews of earlier results exist[7-13] and partly because I am more familiar with our own work.

I. EXPERIMENTAL TECHNIQUES

Aside from bandwidth improvements in digital correlator designs,[15] recent advances include accessibility of light scattering measurements to small scattering angles[18,19] and improvements of complementary techniques in fluorescence photobleaching recovery (FPR)[29] and forced Rayleigh scattering (FRS).[22-24] In particular, a small angle light scattering prism cell and the use of a moving Ronchi grating in FPR will be discussed.

1. *Small Angle Light Scattering Prism Cell*

In dilute polymer solutions, by combining measurements of angular distribution of absolute scattered intensity with Rayleigh linewidths we are able to measure the weight-average molecular weight M_w, the z-average radius of gyration $\langle R_g^2 \rangle_z$, the second virial coefficients A_2 and k_d, and the "z-average" hydrodynamic radius, $\langle R_h^{-1} \rangle_z^{-1}$ using the

expressions based on $S(K) \sim R_{vv}(K)$ and $S(K, \omega)$:

$$\frac{HC}{R_{vv}(K,C)} = \left(\frac{1}{M_w} + 2A_2C\right)[1 + (1 + 2A_2M_wC)^{-1}\langle R_g^2\rangle_z K^2/3] \quad (1)$$

$$\langle R_h^{-1}\rangle_z^{-1} = k_BT/(6\pi\eta\langle D^0\rangle_z) \quad (2)$$

where

$$\langle D_z\rangle = \sum N_i M_i^2 D_i / \sum N_i M_i^2$$

and

$$\langle \Gamma\rangle [\equiv \langle D^0\rangle_z (1 + k_dC)K^2] = \int \Gamma G(\Gamma) d\Gamma$$

with $G(\Gamma)$ being the normalized linewidth distributions; $\Gamma (\equiv \tau_c^{-1})$, the characteristic linewidth or the reciprocal of the characteristic decay time τ_c; η, the solvent viscosity; k_B, the Boltzmann constant; and, N_i, the number of molecules of species i. In eq 2, we have assumed that measurements of the z-average translational diffusion coefficient $\langle D\rangle_z$ satisfies the condition $KR < 1$ with R being a characteristic length. For random coils, with $KR_g < 1$ the particle scattering factor [or the static structure factor $S(K)] \sim 1$. At higher scattering angles, as K is increased, internal molecular motions begin to contribute to $\langle \Gamma\rangle$ with a leading term proportional to K^4:

$$\langle \Gamma\rangle = \langle D\rangle_z K^2 (1 + f\langle R_g^2\rangle_z K^2 + \cdots) \quad (3)$$

where f is a dimensionless number depending upon chain structure, polydispersity and solvent power.[17] Thus, if we were trying to avoid the complications introduced by eq 3, we need to make linewidth measurements at small scattering angles whenever the polymer size becomes large. Figure 1 shows a schematic diagram of such a prism light-scattering cell[18] which can measure the angular distribution of excess absolute scattered intensity, $R_{vv}(K)$, down to a scattering angle θ of $\sim 4°$. The main advantages of the prism cell are as follows.

(1) It permits simultaneous measurements of light scattering intensity and time correlation function. Therefore, we have access to determinations of A_2, M_w, $\langle R_g^2\rangle_z$, $\langle R_h^{-1}\rangle_z^{-1}$ and k_d in dilute solutions of very high molecular weight polymers with molecular weights $\lesssim 10^8$. Precise measurements of the intensity time correlation function, $G^{(2)}(K, \tau)$,

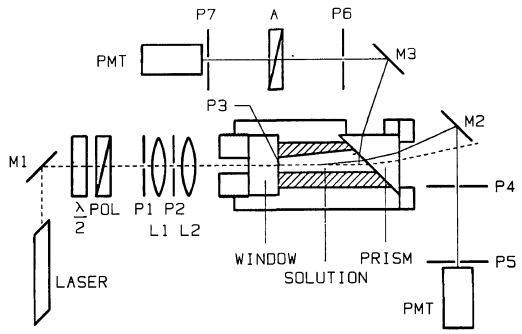

Figure 1. Schematic diagram of a prism light scattering spectrometer. Laser, Spectra Physics model 124 HeNe laser, $\lambda_0 = 632.8$ nm operating at 10 mW; M-1, 2, 3, dielectric mirrors; P-1, ···7, pinholes; L-1, 2, lenses. Total angular divergence $\delta\theta = 0.2°$ at small scattering angles, and $\delta\theta = 0.3°$ at large scattering angles.

permit us to estimate the characteristic linewidth distribution $G(\Gamma)$ by means of a Laplace inversion

$$|g^{(1)}(\tau)| = \int_0^\infty G(\Gamma) e^{-\Gamma\tau} d\Gamma \quad (4)$$

where, in the self-beating mode, $G^{(2)}(K, \tau) = A(1 + b|g^{(1)}(K, \tau)|^2)$ with A and b being the respective background and spatial coherence factor. Access of dynamic linewidth measurements at small and large scattering angles also provides us with an experimental approach to separate the characteristic decay time due to translation from those due to internal motions.

(2) The temperature-controlled light-scattering prism cell has an effective small cell volume which is a contiguous part of a capillary flow system. Therefore, such a cell can be adapted as a detector for size exclusion chromatography. The essential features of the prism light scattering cell are its two accessible surfaces of the prism as exits for the scattered light and the use of the prism as a reference in differential refractometry whereby the refractive index of the solution is measured by relative changes in the direction between the incident and the transmitted laser beam.

Other developments for light-scattering spectrometers using optical fibers[19] and a time interval digitizer[20,21] have been reported. It should be emphasized that techniques related to photon correlation spectroscopy, either in optical arrangements or in hardware correlator designs, have matured. Routine commercial instruments exist.

Nevertheless, we should also realize that there have been recent developments in related experimental techniques which can be used to study polymer dynamics.

2. *Advances in Fluorescence Photobleaching Recovery (FPR) and Forced Rayleigh Scattering (FRS)*

Complementary methods such as forced Rayleigh scattering[22-24] (or holographic relaxation spectroscopy (HRS)) and fluorescence photobleaching recovery[25,26] are capable of measuring translational diffusion coefficients many orders of magnitude smaller ($\sim 10^{-12}$ cm^2 s^{-1}) than photon correlation spectroscopy. Although FPR and FRS (or HRS) require the use of respective fluorescent and photochromic probe molecules, the probes have the advantage of selectivity, *i.e.*, observing only systems of interest by design. There are experimental complications associated with both techniques. However, in FPR, the introduction of periodic pattern photobleaching[26,27] and of a scanning detection system[28] has simplified both theory and practice as well as improved the signal processing technique. Lanni and Ware[29] combined the simplicity of the periodic pattern photobleaching with the scanning detection and were able to virtually eliminate sensitivity due to long-term motion of the specimen and data distortion due to continued photobleaching by the monitoring beam. Furthermore, the decay at the fundamental frequency is observed in real time and the measurement is insensitive to dc drift components. In FPR, a small fraction of the probe molecules is decomposed while in HRS, which was pioneered by Pohl *et al.*[30] and Eichler *et al.*,[31] the probe molecules are not destroyed. In their initial scheme, Pohl *et al.* used two intersecting coherent pulsed laser beams to induce a transient thermal grating in a slightly absorbing medium and measured thermal diffusivity by monitoring the decay of the reading beam, as diffracted by the thermal grating which was gradually smeared out by thermal diffusion. By using photochromic dye molecules, a periodic concentration grating of photoexcited dye molecules is created.[22-24] If the dye molecules are attached to macromolecules, the self-diffusion behavior of labelled chains is observed provided that there is no concentration dependence of the labelled dye on the observed relaxation time. Applications of FPR and FRS to studies of polymer solutions in semidilute and concentrated regimes as well as of gels will undoubtedly play an important role because of specificity and dynamic range made available by such techniques even though we must be careful to pay particular attention to the chemistry of photochromic[32] and fluorescent probes.

3. *Laplace Inversion*

Equation 4 is a Fredholm integral equation of the first kind. The problem associated with recovering the normalized characteristic linewidth distribution function $G(\Gamma)$ is due to the ill-conditioned nature of eq 4 since the experimental data, $|g^{(1)}(\tau)|$, is bandwidth limited and contains noise. There have been chapters of two recent books dealing specifically with the linewidth polydispersity analysis.[33,34] By means of eq 4 the amount of information about $G(\Gamma)$ which can be recovered from bandwith limited and noisy $|g^{(1)}(\tau)|$ is limited. Essential mathematics allowing implementation of the singular value decomposition technique and a linearized method of regularization have been described.[16]

In the singular value decomposition technique, we first introduce a reasonable and mathematically tractable initial approximation for $G(\Gamma)$, such as

$$G(\Gamma)=\sum_{i=1}^{N} P_i\delta(\Gamma-\Gamma_i) \tag{5}$$

where the Dirac delta functions form an N sum of fixed discrete characteristic linewidths, Γ_i's with amplitudes, P_i's, which are determined by a linear least squares fitting procedure. In matrix form,

$$CP\simeq b \tag{6}$$

where C is the $(m\times n)$ curvature matrix with $c_{ij}=e^{-\Gamma_j\tau_i}$, P is the parameter vector of length n, and b is the data vector of length m with $b_i=g^{(1)}(\tau_i)$. The symbol $\simeq$ indicates solution in a least-squares sense. Prior to entering the singular value decomposition routine,[35] the columns of C are scaled to unit norm in order to improve the numerical stability of the inversion. We have

$$Ax\simeq b \tag{7}$$

where $A=CH$, $x=H^{-1}P$, and

$$h_{ij}=\left(\sum_{j=1}^{n} c_{ij}^2\right)^{1/2}\delta_{ij}.$$

Equation 7 is decomposed by orthogonal transfor-

mations to the equivalent problem

$$USV^{-1}x \simeq b \tag{8}$$

with U and V^{-1} being orthogonal matrices and S being a diagonal matrix whose non-zero elements are monotonically decreasing. By defining $x=Vy$ and $U^{\mathrm{T}}b=g$, we have

$$Sy \simeq g \tag{9}$$

which yields

$$y_{\mathrm{i}}=g_{\mathrm{i}}/s_{\mathrm{i}} \tag{10}$$

with s_i being the ith singular value, S_{ii}. The elements of S contain the essential elements of information of eq 6. A rank reduction step is usually employed to limit the amount of information which can be extracted above the noise level of the measured data. We have successfully selected $\boldsymbol{k}$ such that $\|r^{(\boldsymbol{k})}\|$ is sufficiently small without $\|P^{(\boldsymbol{k})}\|$ getting too large where $r^{(\boldsymbol{k})}=CP^{(\boldsymbol{k})}-b$ and $P^{(\boldsymbol{k})}=Hx^{(\boldsymbol{k})}$. The Euclidean norm of a vector z can be computed from $\|z\|=(\sum_i z_i^2)^{1/2}$. In the $y^{(\boldsymbol{k})}$ candidate solutions, we have

$$y^{(\boldsymbol{k})}=\begin{cases} g_i/s_i & \text{for} \quad 1<i\leq \boldsymbol{k} \\ 0 & \text{for} \quad \boldsymbol{k}<i\leq n\,. \end{cases} \tag{11}$$

Following the method of regularization,[16] we use

$$\bar{b}(\tau)=\int_{\Gamma_{\min}}^{\Gamma_{\max}} \boldsymbol{K}(\Gamma,\tau)G(\Gamma)\,\mathrm{d}\Gamma \qquad 0<\tau<\infty \tag{12}$$

as the continuous noise-free data function with $\boldsymbol{K}(\Gamma,\tau)=\mathrm{e}^{-\Gamma\tau}$ and

$$b(\tau)=\bar{b}(\tau)+r(\tau) \tag{13}$$

as the measured data with additive noise $r(\tau)$. In Abbiss *et al.*,[36] a regularized approximation to the true distribution was obtained by minimizing the following functional:

$$F(u)=\|b-\boldsymbol{K}u\|^2+\alpha\|Ju\|^2 \tag{14}$$

where α is the regularization parameter and J is taken to be the identity operator. The solution to $[\boldsymbol{K}^*\boldsymbol{K}+\alpha J^*J]\tilde{G}=\boldsymbol{K}^*b$ is

$$\tilde{G}=[\boldsymbol{K}^*\boldsymbol{K}+\alpha J^*J]^{-1}\boldsymbol{K}^*b \tag{15}$$

where the asterisk denotes the adjoint operator. The N^{th} iteration estimate of $\tilde{G}$ has the form:

$$\tilde{G}^{(N)}=\boldsymbol{K}^*b+[(1-\alpha)I-\boldsymbol{K}^*\boldsymbol{K}]\tilde{G}^{(N-1)} \tag{16}$$

In the two approaches, the singular value decomposition technique which has been coupled with the use of eq 5 can retrieve the optimum information on $G(\Gamma)$ without additional constraints such as positivity, while we have taken an identity operator for J in order to retain linear techniques for the method of regularization. There are other approaches to the method of regularization, such as Fisher's test used by Provencher[37] with origin from the Tikhonov regularization.[38]

The Laplace inversion problem can be refined further. In order to optimize the amount of information which can be retrieved, it is important to understand the physical basis and limitations related to the constraints which can be incorporated into the regularization parameters, *i.e.*, the more we know the system, the more information we can retrieve from a given set of bandwidth limited measured data which contain noise. Thus, the Laplace inversion becomes one of the linkages among measurements, analysis, model and theory. It is a part of the iterative procedure which must be incorporated into the experiment. With appropriate signal-to-noise ratio and a sufficiently broad frequency range for the measured time correlation function which spans the lower and upper bounds of the characteristic time distribution function, we can indeed retrieve more information than the usual average linewidth $\bar{\Gamma}$ and its variance $\mu_2/\bar{\Gamma}^2$, without an *a priori* assumption on the form of $G(\Gamma)$.

II. APPLICATIONS TO POLYMER SOLUTIONS AND MELTS

1. *Dilute Solution Regime*

In dilute solutions where polymer coils are not entangled, $|g^{(1)}(\tau)|$ permits us to estimate the molecular weight distribution and to determine the hydrodynamic radius when $KR<1$ and to investigate internal motions when $KR\gg 1$.

A. *Molecular Weight Distribution.*

By combining eq 1, 3, 4, and 5, the unnormalized weight molecular weight distribution $F_w(M)$ has the form:

$$\begin{aligned} F_w(M)&=\sum_j C_j\delta(M-M_j) \\ &=\sum_j (P_j^{\mathrm{o}}/M_j)\delta(M-M_j) \end{aligned} \tag{17}$$

where we have set $P_j^0[=N_jM_j^2=C_jM_j]$ being the scattering amplitude at infinite dilution and zero

scattering angle. At finite concentration and scattering angle,

$$P_j^+ \simeq C_j M_j P(KR_{g,j})/(1+2A_2M_wC) \quad (18)$$

and

$$\Gamma_j \simeq D_j^0(1+k_dC)K^2[1+fR_{g,j}^2(1+2A_2M_wC)^{-1}K^2] \quad (19)$$

where we can accept the approximations that A_2 and k_d are relatively independent of the molecular weight over limited ranges of $F_w(M)$ and f, in dilute solutions. With $D^0=k_DM^{-\alpha_D}$, we can compute the molecular weight distribution from laser light scattering measurements. From eq 18 and 19, we have two extrapolations based on eq 5. On the intensity (P_j^+) axis, we have

$$1/P_j^+ \simeq 1+(f+1/3)R_{g,j}^2(C)K^2+O(K^4) \quad (20)$$

where we have set $\int G^+(D^*)\mathrm{d}D^* \sim R_{vv}(K)$ with $G^+(D_j^*)[\equiv P_j^+]$ and D_j^* being the unnormalized scattered intensity of the j^{th} representative fraction and Γ_j/K^2, respectively. On the characteristic linewidth (Γ) axis, we have

$$D_j^* = \Gamma_j/K^2 = 1+fR_{g,j}^2(C)K^2 \quad (21)$$

where $R_{g,j}^2(C=0) \simeq R_{g,j}^2(C)(1+2A_2M_wC)$. By combining eq 20 and 21, we can estimate f and $R_{g,j}^2$ as well as P_j^+ values.

As an illustration, a determination of molecular weight distribution (MWD) of PPTA or Kevlar is shown in Figure 2. The details have been described elsewhere.[39-41] It should be noted that PPTA is soluble mainly in sulfonic acids which are highly corrosive and that the polyelectrolytes may exhibit long-range electrostatic interactions. With experimental values of R_g, f, A_2, k_d, and k_D, which remain essentially constant for a given polymer-solvent system, we can determine the MWD of PPTA in 96% H_2SO_4 plus 0.05 M K_2SO_4 using one time correlation function measured at one fixed scattering angle (*e.g.*, $\theta=45°$) and concentration (*e.g.*, $c=2.8\times10^{-4}$ g ml^{-1}). Figure 2(a) shows a typical plot of $|g^{(1)}(t)|$ *versus* delay time t for the PPTA solution. The corresponding $G(\Gamma)$ as shown in Figure 2(b) can be determined using methods described in Section I.3. In our case, $G(\Gamma)$ was obtained by the singular value decomposition technique [eq 5—11]. Using the procedures outlined in Section II.1.A, we could obtain a MWD for PPTA with $M_w=4.26\times10^4$ g mol^{-1} and $M_z : M_w : M_n = 6.2 : 1.8 : 1$ as

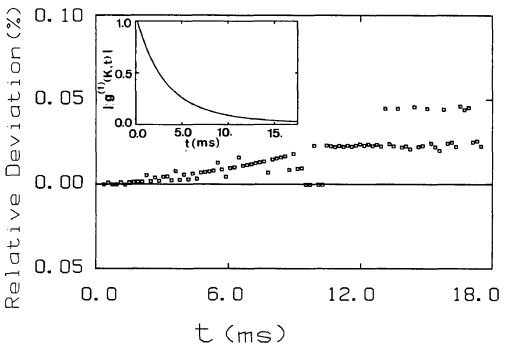

Figure 2(a). Plot of relative deviation in $|g^{(1)}(\tau)|$ for the two characteristic linewidth distributions: $G(\Gamma)$ with and without the 1% shaded section. The shaded contribution of $G(\Gamma)$ corresponds to a base-line adjustment of ~0.05%. A plot of $|g^{(1)}(\tau)|$ *versus* τ is inserted to demonstrate the precision required in the time correlation function measurements, *i.e.*, the fittings can always be achieved such that the measured and the computed $|g^{(1)}(\tau)|$ are indistinguishable within the experimental error limits. Measured and computed base-line must agree within ~0.1%.

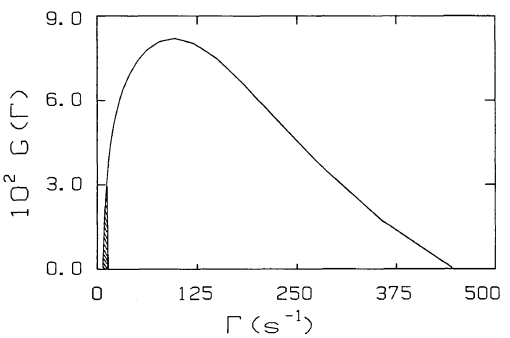

Figure 2(b). Plot of $G(\Gamma)$ *versus* Γ. The shaded area represents 1% of the area of $\int G(\Gamma)\mathrm{d}\Gamma$.

shown in Figure 2(c). In the molecular weight transform, we have used $D^0=2.07\times10^{-5}M^{-0.75}$ with M expressed in g mol^{-1}, $A_2=3.23\times10^{-3}$ cm^3 mol g^{-2}, $k_d=60$ cm^3 g^{-1}, $\delta=0.2$ and $\langle R_g^2\rangle_z^{1/2} \sim 35$ nm where δ is the molecular anisotropy. For PPTA solutions, eq 18 and 19 need to be modified because of molecular anisotropy:

$$R_g^2(0) = [(1+4\delta^2/5)/(1-4\delta/5+4\delta^2/7)] \times [1+2A_2M_wC/(1+4\delta^2/5)]R_{g,app}^2 \quad (22)$$

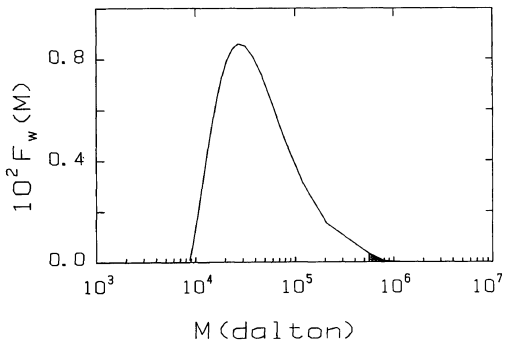

Figure 2(c). Molecular weight distribution of PPTA based on $G(\Gamma)$ from Figure 2(b). The shaded area represents the baseline uncertainty in the time correlation function measurement which can be translated to uncertainties in the high molecular weight tail. $F_w(M)$ is the weight distribution.

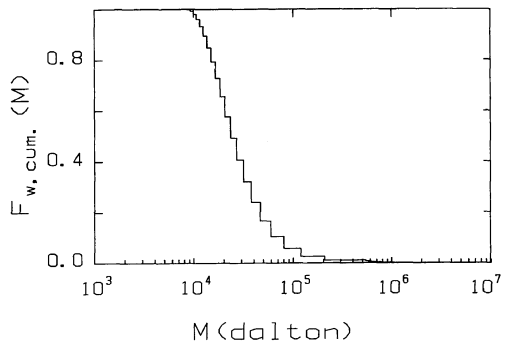

Figure 2(d). Cumulative molecular weight distribution of PPTA from Figure 2(c). Molecular weight fractions vary from 10^4 to $\sim 5\times 10^5$. The high molecular weight tail corresponding to polymers with $M>5\times 10^5$ is seen as within the experimental error limits.

$$F_{w,cum}=\int_{\infty}^{M} F_w(M)M\mathrm{d}M \Big/ \int_{\infty}^{0} F_w(M)\mathrm{d}M$$

At $M>5\times 10^5$ g mol^{-1}, the amount of polymer in $F_{w,cum}$ has become negligibly small.

$$M_{app}=M_w(1+4\delta^2/5) \qquad (23)$$

where $R^2_{g,app}$ denotes the effective radius of gyration at finite concentrations without the δ correction.

In the data analysis, it is particularly important to realize the need for precise baseline measurements. A 0.1% baseline fluctuation can be translated to $\gtrsim 1\%$ of $\int G(\Gamma)\mathrm{d}\Gamma$ in the low frequency limit of the characteristic linewidth distribution as shown by the shaded area of $G(\Gamma)$ in Figure 2(b). The corresponding uncertainty in MWD is illustrated by the shaded area in Figure 2(c). Thus, if there is a high molecular weight tail with weight fractions corresponding to ~ 0.01 and $M>5\times 10^5$g mol^{-1}, the light scattering method cannot be used to confirm either its presence or its absence, unless we are able to improve our experimental precision another order of magnitude, which is unlikely. Nevertheless, determinations of MWD by laser light scattering have unique advantages, *i.e.*, the technique is noninvasive, the measurements can be performed in a closed system, and the Laplace inversion, although delicate, has a solid mathematical foundation. Since it can readily be used to determine MWD's of polymers such as polyacrylamide,[42] polyphosphazine,[43] polyethylene[44,45] and PPTA,[39-41] its eventual utilization as an analytical tool, especially for speciality polymers, is expected. Furthermore, its utility as a detector for chromatography cannot be overemphasized.

B. *Coil-Globule Transition*

Another area of interest is the coil-globule transition.[11,45] The temperature and molecular weight dependence of the hydrodynamic radius R_h of polystyrene with M_w varying from 3.8×10^6 to 20.6×10^6 dissolved in two different solvents, cyclopentane and cyclohexane, have been studied by analytical ultracentrifugation.[46] All data can be represented on a single master curve in a plot of the expansion factor $\alpha_h[\equiv R_h(T)/R_h(\theta)]$ *versus* the reduced variable $N/N_\tau = M_w|\tau|^2/(n\alpha M_0)$ where $|\tau| = |1-\theta/T|$ and $n\alpha M_0$ is an adjustable parameter $\simeq 150\pm 30$ g mol^{-1}. In the θ-domain ($N/N_\tau<3$), $\alpha_h\sim 1$. In the collapsed domain ($N/N_\tau>20$), α_h varies as $M_w^{-1/6}|\tau|^{-1/3}$ and $R_h\sim M_w^{1/3}$.

The intrinsic viscosity $[\eta]$ ($\sim R^3/M$) is related to the particle volume. Therefore, viscometry should be a more sensitive technique than quasielastic light scattering (where $D\sim R_h^{-1}$) in evaluating the globule-coil transition behavior. However, the specific viscosity defined as $\eta_{sp}=(\eta/\eta_0)-1$, requires a differential or ratio measurement of viscosity of the solution η and that of the solvent η_0. In the collapsed domain, highly dilute solutions must be used[11] so that the difference between η and η_0 are necessarily quite small. Nevertheless, viscosity measurements with sensitivity approaching ± 0.01 sec or $\delta\eta/\eta\sim 10^{-4}$ are feasible,[47] even though at high molecular weights ($M\gtrsim 10^7$) and extremely low

concentrations ($C \lesssim 10^{-7}$g cm^{-3}), further improvements in precision in the absence of shear rate dependence become desirable.

Light scattering can measure both R_g and R_h. With photon correlation and photon counting it appears to be a good technique to study the coil globule transition. Indeed, many studies have been reported.[48-53] A comparison of the literature data[46] shows two notable exceptions on the hydrodynamic radius in attempts to reach the collapsed regime by using light scattering.[51-53] In particular, the α_h variation in the large N/N_τ region is much too rapid for the Prague group.[53] Although they tried to take advantage of the high viscosity of dioctyl phthalate as their solvent, the same advantage may become a difficulty in reaching the required thermodynamic equilibrium. The discrepancy of the sedimentation data with the MIT group is only qualitative. Nevertheless, light scattering experiments studying the coil globule transition using a range of narrow molecular weight distribution polymers should be repeated especially in approaching and reaching the collapsed domain. Extension of such investigations using star polymers would also be very interesting.

C. *Internal Motions*

Analysis of internal motions in dilute polymer solutions has remained to be a difficult problem[11] because the dynamic structure factor is model dependent. A more generalized approach based on the first cumulant of $g^{(1)}(K, \tau)$ by Akcasu *et al.*[54,55] and Han and Akcasu[56] suggests that eq 3 is an extremely useful expression to experimentally account for internal motions of polymers in solution. More detailed analysis on translational diffusion and internal motion of high molecular weight polystyrenes in benzene at infinite dilution has been reported.[57] In view of the Laplace inversion problem, analysis by the histogram method can only be accepted with caution, especially when the scattering amplitudes of two closely spaced bimodal characteristic linewidth distributions are very different. Furthermore, the bimodal form must break down at large values of KR since high order intramolecular motions become appreciable when $KR \gg 1$.

2. *Semidilute Solution Regime*

In semidilute solutions, two characteristic decay times, in terms of D_c and D_{slow}, have been observed when $KR < 1$. The slow mode was identified incorrectly as the self-diffusion coefficient of a single polymer chain reptating through the entangled polymer coils. However, its molecular weight and concentration dependence, nevertheless, mimics those of the self-diffusion coefficient. Consequently, its behavior could probably be related to reptation of a clustering of polymer chains through the entangled coils. The cluster concept came about because $D_{slow} \ll D_s$.

Polymer self-diffusion in entangled systems has been reviewed by Tirrell[58] who has listed 277 references. The extensive review is instructive and contains a lucid account of the present status. Dynamics of entangled systems has been reviewed by Graessley,[59] and of the reptation model[60] by de Gennes[61] and others.[62,63] The polymer chain moving along the contour of the tube[64] made up of neighboring polymer chains has a "tube diffusion coefficient," D_{tube}:

$$D_{tube} = k_B T M_0/(\zeta_0 M) \tag{24}$$

where M_0 and ζ_0 are the molecular weight of a monomer unit and the monomer friction coefficient, respectively. The polymer chain of length $L(\equiv bM/M_0)$ will escape from its tube over a time τ such that $D_{tube} = L^2/2\tau$ or

$$\tau_c = L^2/2D_{tube} \sim M^3 \tag{25}$$

and

$$D_s \sim R_g^2/\tau_c \sim M^{-2} \tag{26}$$

The concentration dependence of D_s can be formulated from $D_s(C, M) = D_s(0, M)(C/C^*)^x$ where $C^*(\sim M^{1-3\nu}$ with $R_g \sim M^\nu)$ is the overlap concentration. As $D_s(C, M) \sim M^{-2}$, $D_s(0, M) \sim R_g^{-1} \sim M^{-\nu}$, we have

$$D_s(C, M) \sim M^{-2} C^{(\nu-2)/(3\nu-1)} \tag{27}$$

yielding $D_s \sim C^{-7/4} M^{-2}$ for $\nu = 3/5$ in a good solvent and $D_s \sim C^{-3} M^{-2}$ for $\nu = 1/2$ in a theta solvent. The scaling behavior of eq 27 is expected to hold only over limited ranges of concentration. Equation 27 is further complicated by the influence of multiple length scales.[65,66]

Many experimental techniques including FPR[25-29] and FRS[22-24] have been used to measure self-diffusion coefficients of entangled polymer systems. In addition to FPR and FRS, a listing of the techniques such as NMR,[67] neutron scattering,[68] radioactive tracer,[69] infrared spectroscopy,[70] elec-

tron microscopy,[71] and Rutherford back scattering[72] have been summarized in Table I of reference 58 by M. Tirrell. In quasielastic light scattering (QELS), the slow mode diffusion coefficient D_{slow} mimics, but is smaller in magnitude than, the self-diffusion coefficient.[11,73] Ternary isorefractive QELS uses an isorefractive polymer-solvent pair to measure the self-diffusion coefficient of a trace amount of a miscible, "visible" second polymer.[74,75] It does not require the introduction of probe molecules as in FPR and FRS, but has limited applicability because few miscible polymer pairs with one of which being isorefractive to the solvent exist. Further studies on the slow mode are needed before we can have a clearer concept on its origin as to why it mimics, but is slower than, the self-diffusive motions of a single polymer coil.

One of the practical experimental difficulties in light-scattering studies of polymer solutions in the semidilute regime is the preparation of homogeneous dust-free solutions which become highly viscous at high concentrations. We have succeeded in preparing such solutions by taking advantage of thermal polymerization processes.[73] During the thermal polymerization of methyl methacrylate MMA, we have been able to investigate both the static and dynamic properties of polymethyl methacrylate PMMA dissolved in MMA. As MMA can be clarified readily, we can prepare a dustfree, homogeneous polymer solution at concentrations beyond the usual concentration ranges made available by dissolving a polymer in a solvent. From eq 1, we have

$$\lim_{K\to 0}\frac{HC}{R_{VV}}=\frac{1}{RT}\left(\frac{\partial\pi}{\partial C}\right)_{T,P} \tag{28}$$

where $(\partial\pi/\partial C)_{T,P}$ is the osmotic compressibility. With the polymer concentration detected by Raman spectroscopy, Figure 3 shows a log–log plot of $M(\partial\pi/\partial C)/RT$ *versus* C/C^* for PMMA in MMA. The universal curve starts at values slightly higher than 1 in dilute solutions, shows a broad cross-over region and eventually approaches theta behavior with a slope of 2. The results are in reasonale agreement when we repeat our studies using narrow molecular weight distribution PMMA dissolved in MMA,[76] as shown by hollow circles in Figure 3. There is a small polydispersity effect.[77] The universal curve holds for narrow molecular weight distribution polystyrene of different molecular

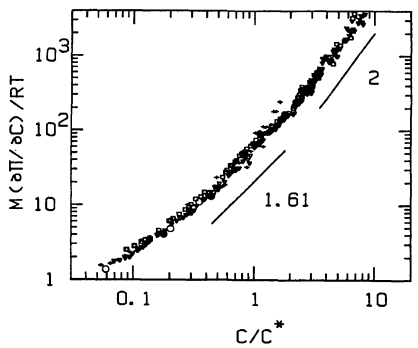

Figure 3. Log-log plot of $M(\partial\pi/\partial C)/RT$ *versus* C/C^* with $C^*=M/(N_A R_g^3)$ for PMMA ($M_w/M_n\sim 2$) in MMA.

Symbol	$10^{-6}M_w$	R_g	$10^2 C^*$	Temp
	g mol^{-1}	nm	g cm^{-3}	°C
Thermal polymerized PMMA				
Plus signs	2.00	52.2	2.33	90
Hollow squares	3.70	74.5	1.49	50
Inverted hollow triangles	4.54	84.5	1.24	50
Prepolymerized PMMA				
Large hollow circles	2.36	—by interpolation—		
Large solid circles	0.08			

weights in toluene and methyl ethyl ketone.[78] In addition to $M(\partial\pi/\partial C)/RT$, the reduced length ξ/R_g is also a universal function of C/C^*, independent of molecular weight or solvent quality where ξ is the static correlation length obeying

$$S^{-1}(K)\sim(\partial\pi/\partial C)_{T,P}(1+\xi^2K^2+O(\xi K)^4 \tag{29}$$

However, the reduced dynamic length[79] ξ_h/R_h is a universal function of k_dC, instead of A_2C which is related to the reduced concentration C/C^*. ξ_h is the dynamic correlation length obeying eq 2 with $\langle D^0\rangle_z$ being replaced by $\langle D\rangle_z=\lim_{K\to 0}\langle\Gamma\rangle/K^2$ for the high-frequency component of the time correlation function (expressed in terms of D_c) in the absence of the slow mode (D_{slow}). Theories of cross-over behavior of the osmotic compressibility and reduced static length ξ/R_g in semidilute polymer solutions in a good solvent have been developed.[77,80-82] For dynamic properties less is known but further theoretical developments are forth-

coming. It should be noted that in the evaluation of $(\partial\pi/\partial C)_{T,P}$, ξ and ξ_h in semidilute solutions, the presence of two modes, due to cooperative (D_c) and "self-diffusive" (D_{slow}) motions, could influence the interpretation of the proposed universal curves. At this time, there is good agreement on the cooperative diffusion coefficient. The slow mode requires further studies. There have been reports suggesting (1) the absence of a slow mode,[79] *i.e.*, quasielastic light scattering sees only the fast mode, (2) a slow mode which is orders of magnitude lower than the fast mode,[83] and (3) a slow mode which is comparable in magnitude to the fast mode.[84,85] The difference in magnitude between D_c and D_{slow} could be related to solvent quality and there are many experiments showing the presence of two modes for polymer solutions in the semidilute regime even though the origin of D_{slow} from quasielastic light scattering is still uncertain. If both modes were present and had comparable amplitude, the composite nature of $(\partial\pi/\partial C)_{T,P}$, ξ and ξ_h could be the source of deviation from the present experimental confirmation on the universal curves, *e.g.*, $\xi(K)$ could depend on polymer coil size in addition to the entanglement correlation length because of the presence of two intensity sources for the excess scattered light.

Light scattering measurements of $(\partial\pi/\partial C)_{T,P}$, R_g, R_h, A_2, and k_d and intrinsic viscosity $[\eta]$ measurements from collapsed to theta and good solvent regimes in dilute solution and of $(\partial\pi/\partial C)_{T,P}$, ξ, and ξ_h for each individual mode as well as η from dilute to semidilute solutions will undoubtedly elucidate our understanding of static and dynamic properties of polymer solutions including entangled systems such as gels and polymer melts. Dynamic measurements in semidilute solutions at $KR>1$ have been ignored so far for lack of comprehensive theoretical models even though we have, in fact, touched upon, but ignored its complexity in evaluating ξ.

3. POLYMER MELTS

A. *Theoretical Background*

Rayleigh–Brillouin and depolarized Rayleigh spectra reveal effects of segmental and orientational motions and cover a broad range of characteristic decay times (10^{-8}—10^{-12} s) which can be frequency analyzed by Fabry-Perot interferometry. At much longer characteristic decay times, *i.e.*, for $1/\Gamma \gtrsim 10^{-6}$ s, the dynamics of slowly relaxing fluctuations in density and optical anisotropy of bulk polymers near the glass transition can be analyzed by photon correlation spectroscopy. For polarized light scattering, the scattered intensity includes both isotropic and anisotropic components, *e.g.*, (at $\theta=90°$) $I_{VV}=I_{iso}+(4/3)I_{VH}$. If $I_{VH}\ll I_{iso}$, $I_{VV}\sim I_{iso}$. So the polarized spectrum of scattered light in a simple viscous fluid, due to longitudinal density fluctuations, has a central Rayleigh peak and two shifted Brillouin peaks where the total scattered intensity is proportional to $\rho k_B T/K_0$ with ρ and K_0 being the mass density and the static modulus of compression, respectively. $K_0=1/\beta_T$ with β_T being the isothermal compressibility. The ratio of the central peak intensity to the total Brillouin intensity $I_C/2I_B$ in the purely viscous limit is $I_C/2I_B=\gamma-1$ where $\gamma(=C_P/C_V)$ is the ratio of the specific heats at constant pressure and volume. The linewidth of the central Rayleigh peak, $\Gamma_R=\kappa K^2/\rho C_P$ with κ being the thermal conductivity. The Brillouin shift $\Delta\omega_l$ is determined by the adiabatic longitudinal sound velocity $v_l(K)$: $\Delta\omega_l=Kv_l(K)$ where $v_l(K=0)=(\gamma K_0/\rho)^{1/2}$ and the Brillouin linewidth, $\Gamma_B=[K^2/(2\rho)](\eta_v+4\eta_s/3)$ with η_v and η_s being the volume and shear viscosities. In simple viscous liquid, relaxing times that contribute toward viscosities are fast compared to $1/\Delta\omega_l$.

For viscoelastic fluids with finite relaxation times which contribute to both elastic and viscous responses, the frequency dependent adiabatic longitudinal modulus $M(=K_0+(4/3)G$ with G being the shear modulus) has the form[12,86]

$$M^*(\omega)=\gamma K_o+M_R\int_0^\infty \frac{\rho(\tau)i\omega\tau}{1+i\omega\tau}d\tau \qquad (30)$$

where M_R is the total relaxation strength for all processes which are coupled to the longitudinal stress and $\rho(\tau)$ is the distribution of relaxation times (τ). With the decrease in I_B, a Mountain peak[87] appears to account for the constant total intensity and $I_C/2I_B$. The shape of the Mountain peak

$$S_M(\omega)=\int_0^\infty \frac{\rho(\tau)\tau}{1+(\omega\tau)^2}d\tau \qquad (31)$$

does not depend on K.

More generally, the time correlation of the isotropic component of the scattered light has the

form:[13]

$$C_{\mathrm{iso}}(K,t)=\alpha^2\left\langle \sum_{m,n}^{N}\sum_{i,j}^{N_S}\exp\{i\boldsymbol{K}\cdot[\boldsymbol{r}_j^{(n)}(t)-\boldsymbol{r}_i^{(m)}(0)]\}\right\rangle \tag{32}$$

where N_S is the number of scattering elements in the chain, $r_j^{(n)}(t)$ is the position of jth element with polarizability α on polymer n at time t in the laboratory-fixed coordinate system. N is the number of polymer chains and the angular brackets denote an ensemble average. Equation 32 has an analytical form only for the high frequency part of density fluctuations in the Rayleigh-Brillouin spectrum. By using a generalized relaxation equation, parameters can be introduced to interpret the VV spectrum.[88] For depolarized light scattering, in the VH geometry,

$$C_{\mathrm{VH}}(\boldsymbol{K},t)=\left\langle \sum_{m,n}^{N}\sum_{i,j}^{N_S}\alpha_{yz}^{(n)}(j,t)\cdot\alpha_{yz}^{(m)}(i,0)\exp\{i\boldsymbol{K}\cdot[\boldsymbol{r}_j^{(n)}(t)-\boldsymbol{r}_i^{(m)}(0)]\}\right\rangle \tag{33}$$

where $\alpha_{yz}^{(n)}(j,t)$ is the yz component of the polarizability tensor of the jth scattering element on the polymer chain n at time t. The HV spectrum has three main features[12] due to (1) scattering by pairs of density fluctuations, (2) direct relaxation of intramolecular orientation fluctuations and (3) coupling between shear and optical anisotropy.

In polarized Rayleigh–Brillouin spectroscopy, multiparameter fittings, including convolution with the instrumental linewidth are often used. The main physical properties which can be obtained from polarized Rayleigh–Brillouin spectra are the Brillouin linewidth Γ_B and the longitudinal sound velocity v_l while for the depolarized Rayleigh spectra, a collective relaxation time $\tau_{or}(\equiv 1/(2\pi\Gamma_{or})$ with Γ expressed in Hz) can be estimated. The difficulties with Fabry–Perot interferometry for studying polymer dynamics are its limited bandwidth range (finesse $\lesssim 10^2$) and precision (frequency linearity $\sim$a few percent). Consequently, in the presence of baseline which cannot be determined independently as in the case of photon correlation spectroscopy, it is not appropriate to attempt a Laplace inversion of the measured spectrum. Even deconvolution of the instrumental linewidth with the measured data in order to obtain the correct spectrum is usually difficult to perform. Rather, the measured spectra are often compared with theoretical spectra which have been convoluted to include the effects of the instrumental function. Thus, the *average* characteristic decay time measured by Fabry–Perot interferometry is particularly susceptible to instrumental bandwidth limitations.

In photon correlation spectroscopy, the broad characteristic time distribution function reveals a very non-single exponential behavior in the time correlation function which has been represented well by an empirical Williams-Watts function:

$$|g^{(1)}(\tau)|=\exp(-t/\tau_0)^{\beta} \tag{34}$$

where $\beta(0<\beta\leq 1)$ is a measure of the characteristic decay time distribution. The mean relaxation time $\bar{\tau}$ is defined by

$$\bar{\tau}=\int_0^{\infty}|g^{(1)}(t)|\mathrm{d}t=(\tau_0/\beta)\Gamma(\beta^{-1}) \tag{35}$$

where $\Gamma(\beta^{-1})$ is the gamma function.

B. *Results*

Results of temperature dependence of relaxation times can best be illustrated by Figure 4 which shows the range of relaxation processes in polyphenylmethyl siloxane (PPMS) as probed by different techniques[13] including photon correlation spectroscopy (PCS),[89] depolarized Rayleigh scattering (DLS),[90] ultrasonic absorption (US), dielectric relaxation (DR) and Brillouin scattering (BS).[91] In

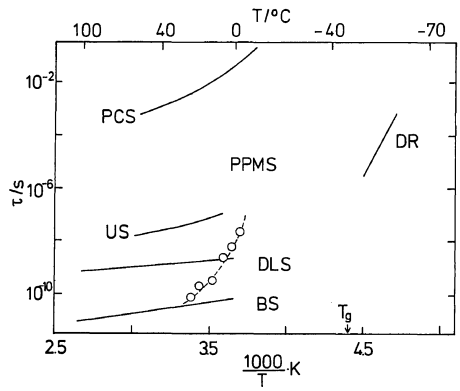

Figure 4. Relaxation processes of polyphenylmethyl siloxane (PPMS) as probed by different techniques including photon correlation spectroscopy[89] (PCS), depolarized Rayleigh scattering[90] (DLS), ultrasonic absorption (US), dielectric relaxation (DR), and Brillouin scattering[91] (BS). The hollow circles are characteristic decay times at 1 atm pressure extrapolated from high pressure measurements using PCS.[92]

addition to the fact that different bandwidth limited physical techniques probe or emphasize different motions, it is quite evident that the dynamics of polymer melts could involve very broad characteristic decay time distributions, so broad that the mean relaxation times are likely to be weighted by the techniques used. Thus, we need to establish relationships on the experimental mean relaxation times covering $\sim 10^{11}$ orders of magnitude and compare them with theory before a detailed understanding of bulk polymer dynamics can be achieved.

In summary, light scattering studies have made advances in the dilute solution regime. A new technique has been developed to characterize polymer molecular weight distributions. Investigations of globule-coil transition have shown inconsistencies with other techniques such as sedimentation and require further study. Internal motions in dilute polymer solutions have been investigated by light scattering. Its usage should complement related techniques such as transient electric birefringence. In semidilute solutions, for $KR<1$, the time correlation function appears to have two modes: a fast cooperative mode and a slow mode. The origin of the slow mode is still open for discussion. It is likely that D_{slow} is not the self-diffusion coefficient. However, more light scattering experiments in combination with FRS and FRP are needed before one can make a definitive conclusion on the origin of the slow mode. When $KR \gg 1$, the complex dynamics has prevented detailed analysis of experiments in semidilute solutions. In bulk polymers, the dynamics reveals a very broad distribution of characteristic decay times which no single physical technique is able to cover. Thus, the mean relaxation times may represent only bandwidth limited and weighted averages of a very broad distribution of characteristic decay times of a single process or very broad distributions of characteristic decay times of different processes. A detailed knowledge of the complex polymer dynamics requires a combined appreciation of experimental limitations and the nature of measured average decay times including introduction of new techniques such as FPR and light scattering photography[93] as well as theoretical developments encompassing those properties.

Acknowledgement. We gratefully acknowledge the National Science Foundation (DMR 8314193), the U.S. Army Research Office, and the Petroleum Research Fund, administered by the American Chemical Society, for support of this research.

REFERENCES

1. L. K. Nicholson, J. S. Higgins, and J. B. Hayter, *Macromolecules*, **14**, 836 (1981).
2. D. M. Mills, *Phys. Today*, **37**, 22 (1984).
3. B. Chu, "Laser Light Scattering," Academic Press, New York, N. Y., 1974.
4. B. J. Berne and R. Pecora, "Dynamic Light Scattering," Wiley-Intersciences, New York, N. Y., 1975.
5. "Photon Correlation and Light Beating Spectroscopy," H. Z. Cummins and E. R. Pike, Ed., Plenum Press, New York, N. Y., 1974.
6. "Photon Correlation Spectroscopy and Velocimetry," H. Z. Cummins and E. R. Pike, Ed., Plenum Press, New York, N. Y., 1977.
7. "Scattering Techniques Applied to Supremolecular and Nonequilibrium Systems," S. H. Chen, B. Chu, and R. Nossal, Ed., Plenum Press, New York, N. Y., 1981.
8. "Application of Laser Light Scattering to the Study of Biological Motion," J. C. Earnshaw and M. W. Steer, Ed., Plenum Press, New York, N. Y., 1983.
9. For example, see "Proceedings of the 5th International Conference on Photon Correlation Techniques in Fluid Mechanics," E. O. Schulz-DuBois, Ed., Springer-Verlag, New York, N. Y., 1983.
10. D. W. Schaefer and C. C. Han, Sandia Report SAND82-0825, April, 1982; to be published in "Dynamic Light Scattering: Applications of Photon Correlation Spectroscopy," R. Pecora, Ed., Plenum Press, New York, N. Y., 1984.
11. B. Chu, "Light Scattering Studies of Polymer Solution Dynamics," *J. Polym. Sci.*, to be published.
12. G. D. Patterson, *Adv. Polym. Sci.*, **48**, 125 (1983); *Ann. Rev. Mater. Sci.*, **13**, 219 (1983); also G. D. Patterson and P. J. Carroll, *J. Polym. Sci., Polym. Phys. Ed.*, **21**, 1897 (1983).
13. G. Fytas, "Applications of Laser Light Scattering to the Study of Molecular Motion in Bulk Polymers," to be published.
14. B. Chu, *Phys. Scripta*, **19**, 458 (1979).
15. K. M. Abbey, J. Shook, and B. Chu, in "The Application of Laser Light Scattering to the Study of Biological Motions," J. C. Earnshaw and M. W. Steer, Ed., Plenum Press, New York, N. Y., 1983, pp 77—87.
16. B. Chu, J. R. Ford and H. S. Dhadwal, in Enzyme Structure, a volume of Methods in Enzymology, C. H. W. Hirs and S. N. Timasheff, Ed., Academic Press, New York, N. Y., to be published.
17. W. H. Stockmayer and M. Schmidt, *Pure Appl. Chem.*, **54**, 407 (1982); M. Schmidt and W. H.

Stockmayer, *Macromolecules*, **17**, 509 (1984).
18. B. Chu, I. H. Park, and J. R. Ford, *Polym. Prepr. Am. Chem. Soc., Div. Polym. Chem.*, **24**, 237 (1983).
19. H. R. Haller, C. Destor, and D. S. Cannell, *Rev. Sci. Instrum.*, **54**, 973 (1983).
20. G. Matsumoto, H. Shimizu, and J. Shimada, *Rev. Sci. Instrum.*, **47**, 861 (1976).
21. N. Nemoto, Y. Tsunashima, and M. Kurata, *Polym. J.*, **13**, 827 (1981).
22. H. Hervet, W. Urbach, and F. Rondelez, *J. Chem. Phys.*, **68**, 2725 (1978); H. Hervet, L. Leger, and F. Rondelez, *Phys. Rev. Lett.*, **42**, 1681 (1979); L. Leger, H. Hervet, and F. Rondelez, *Macromolecules*, **14**, 1732 (1981).
23. D. G. Miles, P. D. Lamb, K. W. Rhee and C. S. Johnson, Jr., *J. Phys. Chem.*, **87**, 4815 (1983).
24. J. A. Wesson, I. Noh, T. Kitano, and H. Yu, *Macromolecules*, **17**, 782 (1984).
25. D. E. Koppel, D. Axelrod, J. Schlessinger, E. L. Elson, and W. W. Webb, *Biophys. J.*, **16**, 1315 (1976).
26. B. A. Smith and H. M. McConnell, *Proc. Natl. Acad. Sci. U.S.A.*, **75**, 2759 (1978).
27. B. A. Smith, W. R. Clark, and H. M. McConnell, *Proc. Natl. Acad. Sci. U.S.A.*, **76**, 5641 (1979).
28. D. E. Koppel, *Biophys. J.*, **28**, 281 (1979).
29. F. Lanni and B. R. Ware, *Rev. Sci. Instrum.*, **53**, 905 (1982); see also J. Davoust, P. J. Devaux, L. Leger, *EMBO J.*, **1**, 1233 (1982).
30. D. W. Pohl, S. E. Schwarz, and V. Irniger, *Phys. Rev. Lett.*, **31**, 32 (1973).
31. H. Eichler, G. Salje, and H. Stahl, *J. Appl. Phys.*, **44**, 5383 (1973).
32. "Photochromism," Techniques of Chemistry, Vol. III, G. H. Brown, Ed., Wiley-Interscience, New York, N. Y., 1971.
33. See "Photon Correlation Spectroscopy of Brownian Motion: Polydispersity Analysis and Studies of Particle Dynamics," in ref 9, pp 286—334.
34. See "Essentials of Size Distribution Measurement," in "Measurement of Suspended Particles by Quasielastic Light Scattering," B. E. Dahneke, Ed., John Wiley & Sons, N. Y., 1983, pp 81—252.
35. C. L. Lawson and R. J. Hanson, "Solving Least Squares Problems," Prentice-Hall, New Jersey, 1974.
36. J. B. Abbiss, C. DeMol, and H. S. Dhadwal, *Optica Acta*, **30**, 107 (1983).
37. S. W. Provencher, *Biophys. J.*, **16**, 27 (1976); *J. Chem. Phys.*, **64**, 2772 (1976); *Makromol. Chem.*, **180**, 201 (1979).
38. A. N. Tikhonov and V. Y. Arsenin, "Solutions of Ill-Posed Problems," V. H. Winston & Sons, Washington, D.C., 1977.
39. Benjamin Chu, Qicong Ying, Chi Wu, James R. Ford, Harbans S. Dhadwal, Renyuan Qian, Jingsheng Bao, Jiyu Zhang, and Chaochou Xu, *Polym. Commun.*, **25**, 211 (1984).
40. Qicong Ying, Benjamin Chu, Renyuan Qian, Jingsheng Bao, Jiyu Zhang, and Chaochou Xu, *Polymer*, to be published.
41. Benjamin Chu, Qicong Ying, Chi Wu, James R. Ford, and Harbans S. Dhadwal, *Polymer*, to be published.
42. A. DiNapoli, B. Chu, and C. Cha, *Macromolecules*, **15**, 1174 (1982).
43. B. Chu and Es. Gulari, *Macromolecules*, **12**, 445 (1979).
44. B. Chu, J. R. Ford, and J. Pope, in "Conference Proceedings of the Society of Plastic Engineers," ANTEC '83, **26**, 547 (1983).
45. C. Williams, F. Brochard, and H. L. Frisch, *Ann. Rev. Phys. Chem.*, **32**, 433 (1981).
46. P. Vidakovic and F. Rondelez, *Macromolecules*, **17**, 418 (1984).
47. R. Perzynski, M. Adam, and M. Delsanti, *J. Phys. (Orsay, Fr.)*, **43**, 129 (1982).
48. E. L. Slagowski, B. Tsai, and D. McIntyre, *Macromolecules*, **9**, 687 (1976).
49. M. J. Pritchard and D. Caroline, *Macromolecules*, **13**, 957 (1980).
50. D. R. Bauer and R. Ullman, *Macromolecules*, **13**, 392 (1980).
51. F. Swislow, S. T. Sun, I. Nishio, and T. Tanaka, *Phys. Rev. Lett.*, **44**, 796 (1980).
52. S. T. Sun, I. Nishio, G. Swislow, and T. Tanaka, *J. Chem. Phys.*, **73**, 5971 (1980).
53. P. Stepanek, C. Konak, and B. Sedlacek, *Macromolecules*, **15**, 1214 (1982).
54. A. Z. Akcasu, M. Benmouna, and C. C. Han, *Polymer*, **21**, 866 (1980).
55. M. Benmouna and A. Z. Akcasu, *Macromolecules*, **13**, 409 (1980).
56. C. C. Han and A. Z. Akcasu, *Macromolecules*, **14**, 1080 (1981).
57. N. Nemoto, Y. Makita, Y. Tsunashima, and M. Kurata, *Macromolecules*, **17**, 425 (1984).
58. M. Tirrell, *Rubber Chemistry and Technology*, **57**, 523 (1984).
59. W. W. Graessley, *Adv. Polym. Sci.*, **16**, 1 (1974).
60. P. G. de Gennes, *J. Chem. Phys.*, **55**, 572 (1971).
61. P. G. de Gennes, *Physics Today*, **36**, 33 (1983).
62. P. G. de Gennes and L. Leger, *Ann. Rev. Phys. Chem.*, **33**, 49 (1982).
63. G. Marrucci, in "Advance in Transport Processes," Vol. 5, A. S. Mujumdar and R. A. Mashelkar, Ed., Wiley, N. Y., 1984.
64. S. F. Edwards, *Proc. Phys. Soc. London*, **92**, 9 (1967).
65. D. W. Schaefer, J. F. Joanny, and P. Pincus, *Macromolecules*, **13**, 1280 (1980).
66. P. T. Callaghan and D. N. Pinder, *Macromolecules*, **17**, 431 (1984).
67. E. von Meerwall, *Adv. Polym. Sci.*, **54**, 1 (1984).
68. J. S. Higgins, K. Ma, L. K. Nicholson, J. B. Hayter, K. Dodgson, and J. A. Semlyen, *Polymer*, **24**, 793 (1983).

69. F. Bueche, W. M. Cashin, and P. Debye, *J. Chem. Phys.*, **20**, 1956 (1952).
70. J. Klein and B. J. Briscoe, *Proc. R. Soc. London, Ser. A*, **365**, 53 (1979).
71. P. Gilmore, R. Falabella, and R. L. Laurence, *Macromolecules*, **13**, 880 (1980).
72. E. J. Kramer, P. Green, and C. J. Palmstrom, *Polymer*, in press (1984).
73. B. Chu and D. C. Lee, *Macromolecules*, **17**, 926 (1984).
74. B. Hanley, S. Balloge, and M. Tirrell, *Chem. Eng. Commun.*, **24**, 93 (1983).
75. T. P. Lodge, *Macromolecules*, **16**, 1393 (1983).
76. B. Chu, D.-C. Lee and K. Sun, "Characterization of PMMA during the Thermal Polymerization of Methyl Methacrylate," Preprints, 1st SPSJ International Polymer Conference (IPC 84), Tokyo, 1984, 23B16, p 145.
77. T. Ohta and Y. Oono, *Phys. Lett.*, **89A**, 460 (1982).
78. P. Wiltzius, H. R. Haller, D. S. Cannell, and D. W. Schaefer, *Phys. Rev. Lett.*, **51**, 1183 (1983).
79. P. Wiltzius, H. R. Haller, D. S. Cannell, and D. W. Schaefer, private communication.
80. T. Ohta and A. Nakanishi, *J. Phys. A: Math. Gen.*, **16**, 4155 (1983).
81. A. Nakanishi and T. Ohta, *J. Phys. A: Math. Gen.*, accepted.
82. K. F. Freed, *J. Chem. Phys.*, **79**, 6357 (1983).
83. E. J. Amis and C. C. Han, *Polymer*, **23**, 1403 (1982).
84. T. Nose and B. Chu, *J. Chem. Phys.*, **70**, 5332 (1979).
85. B. Chu and T. Nose, *Macromolecules*, **12**, 599 (1979); **13**, 122 (1980).
86. S. M. Rytov, *Soviet Phys. JETP*, **31**, 1163 (1970).
87. R. D. Mountain, *J. Res. Natl. Bur. Standards*, **70A**, 207 (1966).
88. Y. H. Lin and C. H. Wang, *J. Chem. Phys.*, **70**, 681 (1979).
89. G. Fytas, Th. Dorfmuller, Y.-H. Lin, and B. Chu, *Macromolecules*, **14**, 1088 (1981).
90. Y.-H. Lin, G. Fytas, and B. Chu, *J. Chem. Phys.*, **75**, 2091 (1981).
91. G. Fytas, Y.-H. Lin, and B. Chu, *J. Chem. Phys.*, **74**, 3131 (1981).
92. G. Fytas, Th. Dorfmuller, and B. Chu, *J. Polym. Sci., Polym. Phys. Ed.*, **22**, 1471 (1984).
93. P. J. Carroll, G. D. Patterson, and S. A. Cullerton, *J. Polym. Sci., Polym. Phys. Ed.*, **21**, 1889 (1983).